



Synthesis and Mechanism of Formation of Non-equilibrium Ag–Ni Nanotubes

Rajesh Kumar Rai¹ · Chandan Srivastava²

Received: 14 October 2020 / Revised: 31 December 2020 / Accepted: 13 January 2021 / Published online: 1 February 2021
© ASM International 2021

Abstract

1D material systems such as Ag–Ni, Ag–Co, Ag–Fe nanowires or nanotubes have tremendous potential for making devices that require the coexistence of electrically conducting and magnetic phases and interfaces. The realization of such microstructures is very challenging essentially due to their high positive mixing enthalpies which makes it difficult to achieve unique non-equilibrium microstructures. In the present exploration, silver–nickel nanotubes were synthesized by adopting the electrodeposition technique. Detailed microstructural characterization of the nanotubes was carried out by using electron microscopy technique. The transmission electron microscopic examinations revealed that the microstructure of the nanotube consisted of nearly spherical, Ag–Ni nanoparticles encapsulated in a Ni-rich amorphous matrix. Ag–Ni nanoparticles exhibited two types of structures. The small-sized particles had single-phase crystal structure, whereas large-sized particles exhibited multiple twinned structure. Mechanism of formation of the nanotube involved the nucleation and subsequent growth of Ag–Ni nanoparticles inside the alumina template. Owing to the twinned structure, few nanoparticles grow larger and decomposed into Ag-rich and Ni-rich clusters that eventually matured to the nanotube.

Keywords Nanotube · Electrodeposition · Electron microscopy

Introduction

One-dimensional nano-solids have important applications in the field of electronics [1], sensors [2], optoelectronics [3], catalysis [4], etc. Among the 1D nano-solids, carbon nanotubes, zinc oxide nanowires/nanotubes, and silicon nanowires are the popularly explored material systems [5]. Other 1D material systems such as Ag–Ni, Ag–Co, Ag–Fe nanowires/nanotubes remain relatively less explored essentially due to their high value of enthalpy of mixing (ΔH^{mix}) which makes it difficult to achieve non-equilibrium microstructures [6, 7]. It is worth mentioning that these systems have tremendous potential for making a device that requires coexistence of electrically conducting and magnetic phases and interfaces.

One of the simplest ways to synthesize non-equilibrium microstructures is electrodeposition technique. Manipulation of operating parameters like current density, temperature, pH, etc., during the electrodeposition process provides the flexibility for tuning the formation kinetics and consequently the material microstructure concerning the realization of non-equilibrium phases [6]. In this work, we provide an electrodeposition-based technique to synthesize Ag–Ni nanotubes with a unique non-equilibrium microstructure. Note that equilibrium phase diagram of Ag–Ni system exhibits negligible solubility between Ag and Ni because of large difference in atomic sizes and high positive enthalpy of mixing [6–8].

Experiment

In the present investigation, template-based electrodeposition technique was used to synthesize the nanotubes. This technique ensures the co-deposition of Ag and Ni metals inside the cylindrical orifice of the alumina template (anodic) from their salt solutions. One end of the template is coated by Ag or Au sputtering and attached to a copper

✉ Rajesh Kumar Rai
rajeshrai.bits@yahoo.in; rajesh.meta@mmit.ac.in

¹ Department of Metallurgical and Materials Engineering, MNIT, Jaipur, India

² Department of Materials Engineering, Indian Institute of Science, Bangalore, India

substrate ($4\text{ cm} \times 3\text{ cm} \times 0.3\text{ cm}$) by adhesive tape. The template attached to the copper substrate is used as working electrode, whereas a platinum foil ($2\text{ cm} \times 2\text{ cm} \times 0.3\text{ cm}$) is used as counter electrode. The electrolyte used for the synthesis consisted of 169 mg of AgNO_3 , 250 mg of $\text{Ni}(\text{NO}_3)_2 \cdot 6\text{H}_2\text{O}$, 350 mg of thiourea, 30 mg of H_3BO_3 , and 100 ml of distilled water. A platinum foil ($2\text{ cm} \times 2\text{ cm} \times 0.3\text{ cm}$) and an anodisc attached to a copper substrate ($4\text{ cm} \times 3\text{ cm} \times 0.3\text{ cm}$) by adhesive tape were used as anode and cathode, respectively. Both electrodes were kept parallel, and inter-electrode distance was maintained at 5 cm. pH of the electrolyte was maintained at 3.6 by adding HNO_3 and NaOH . Figure 1 illustrates the schematic diagram of experimental setup used for the electrodeposition of nanotubes. Electrodeposition was carried out at room temperature and under argon gas atmosphere for 30 min using constant current input of 3 mA. After the electrodeposition, template containing nanotubes was detached from the cathode and was dissolved in 3M NaOH solution for 1 h. The liberated nanotubes were further analyzed.

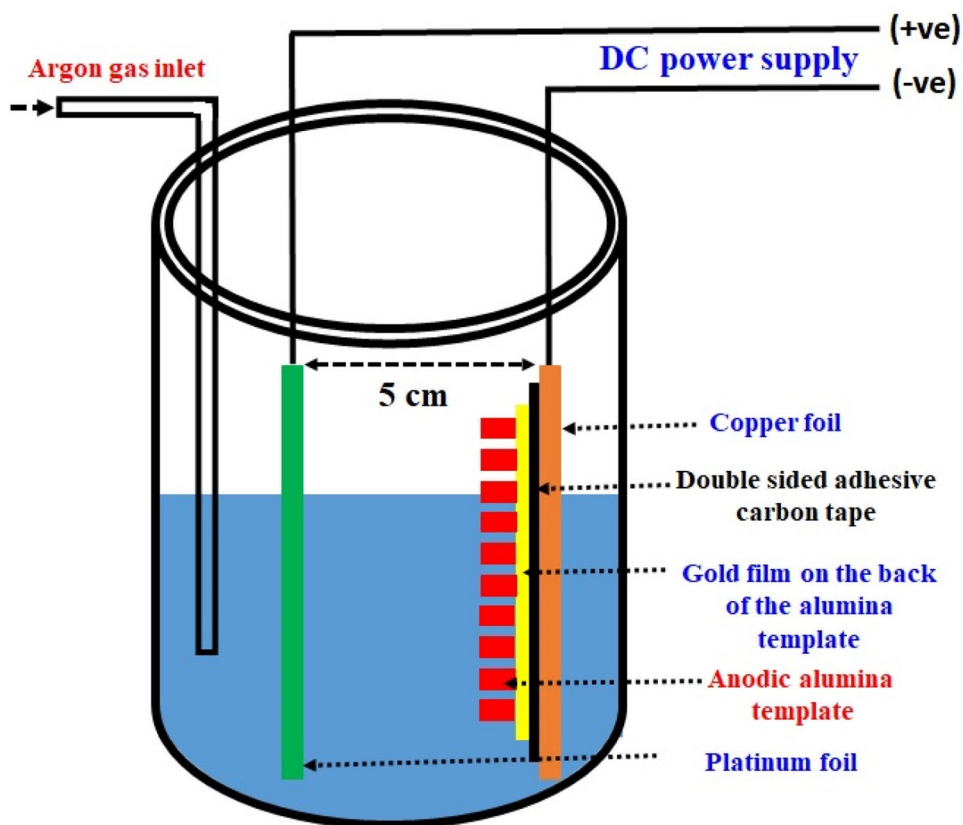
Morphology and composition of the as-deposited samples were determined using a FEG equipped scanning electron microscope (SEM, FEI NOVA Nano SEM 430). FEI Tecnai

F-30 transmission electron microscope (TEM) was used for microstructural characterization of nanotubes. Samples for the SEM- and TEM-based analysis were prepared by dispersion of as-synthesized nanotubes on a silicon wafer and electron transparent carbon-coated Cu grid, respectively. Scanning transmission electron microscopy-energy-dispersive spectroscopy technique was used for obtaining compositional information from individual nanotubes.

Results and Discussion

Figure 2a shows the representative SEM image of electrodeposited mass obtained after the dissolution of the alumina template. It is evident from Fig. 2a that the electrodeposition experiment has produced nearly uniform diameter ($\sim 200 \pm 20\text{ nm}$), high aspect ratio nanotubes. The SEM-EDS analysis was used for the elemental analysis of the nanotubes. SEM-EDS analysis confirmed the presence of Ag and Ni atoms in the nanotubes. TEM bright field images of the nanotubes at different magnifications were captured and are shown in Fig. 2b and c. The nanotube's microstructure consisted of nearly spherical dark nanoparticles distributed in

Fig. 1 A schematic diagram of the experimental setup used for the electrodeposition of nanotubes



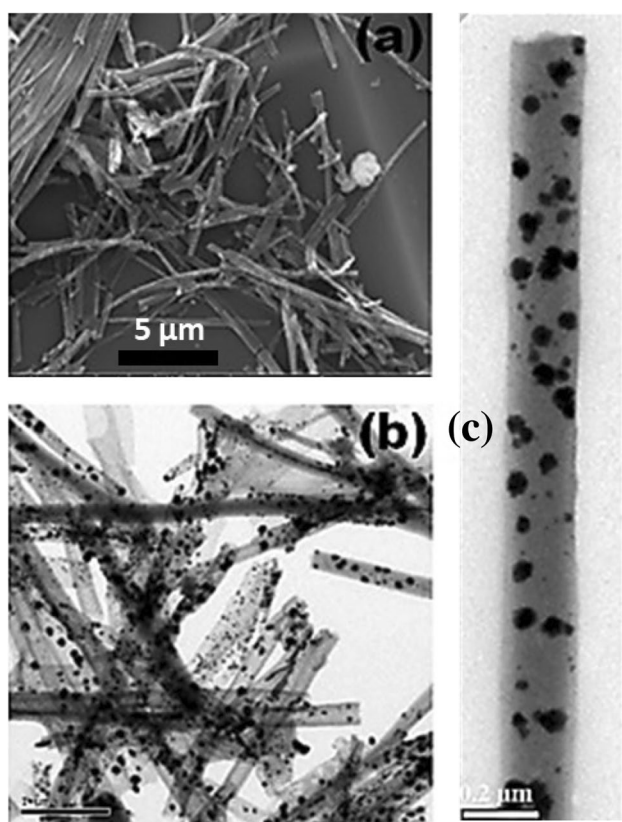


Fig. 2 (a) SEM micrograph of nanotubes, (b) TEM bright field image of nanotubes, (c) higher magnification TEM bright field image of nanotubes

a hollow cylindrical matrix (Fig. 2b and c). The embedded nanoparticles exhibit considerable size variation. Sizes of the nanoparticles were found to be ranging from 10 to 90 nm as represented by size distribution histogram in Fig. 3. It can be seen (Fig. 2a) that a significant fraction of encapsulated nanoparticles has size greater than 30 nm. Such large particles are possibly formed owing to the phase separation. A detailed discussion pertaining to the formation of these large size nanoparticles will be discussed in the ensuing paragraphs.

Compositional identity of the constituent features in the nanotube microstructure was diagnosed by conducting STEM-EDS compositional analysis of the individual growing nanotubes. Figure 4a shows the low magnification STEM image of nanotubes. A magnified view of one such tube (marked by rectangle in Fig. 4a) is shown in Fig. 4b. Figure 4 also confirms the fact that nanotube consists of small size particles (shown by circle in Fig. 4b) as well as large size particles.

The STEM-HAADF image, Ag and Ni compositional maps obtained from nanotubes are provided in Fig. 5a–c, respectively. The contrast generated in the STEM-HAADF image is directly related to the extent of angular scattering of electrons, which in turn depends on the average atomic number along a scanning column in the electron beam direction [9]. A careful observation of the STEM images shows that the contrast within the nanotubes (in the matrix part as shown in Fig. 5a) remains uniform which is a clear

Fig. 3 Size distribution histogram for nanoparticles in the nanotubes

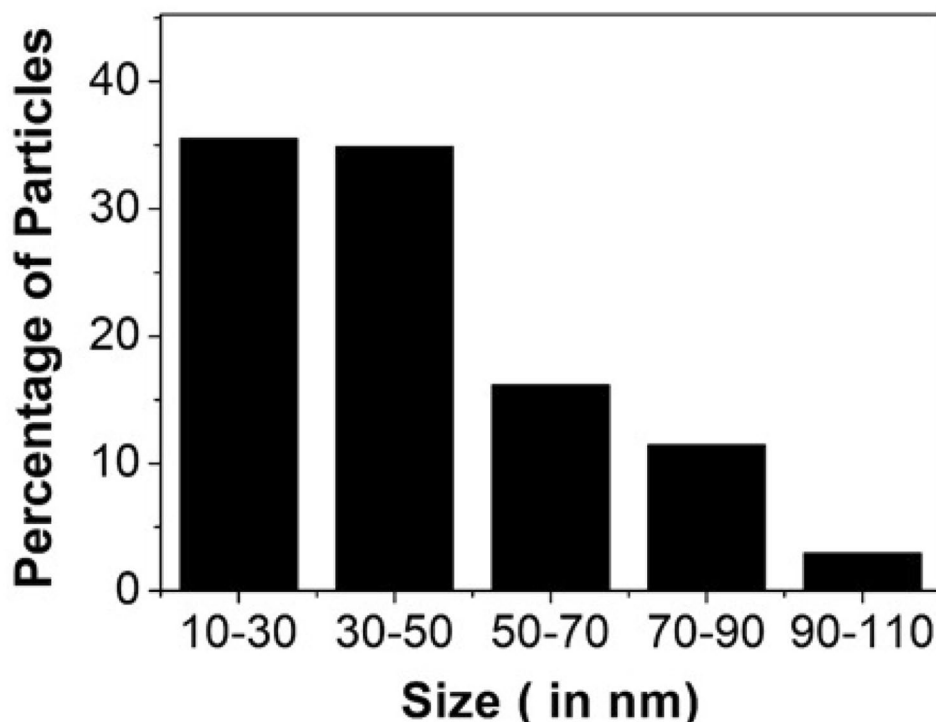


Fig. 4 (a) Low magnification STEM image of nanotubes. A magnified view of one such tube (marked by rectangle in Fig. 3a) is shown in Fig. 3(b)

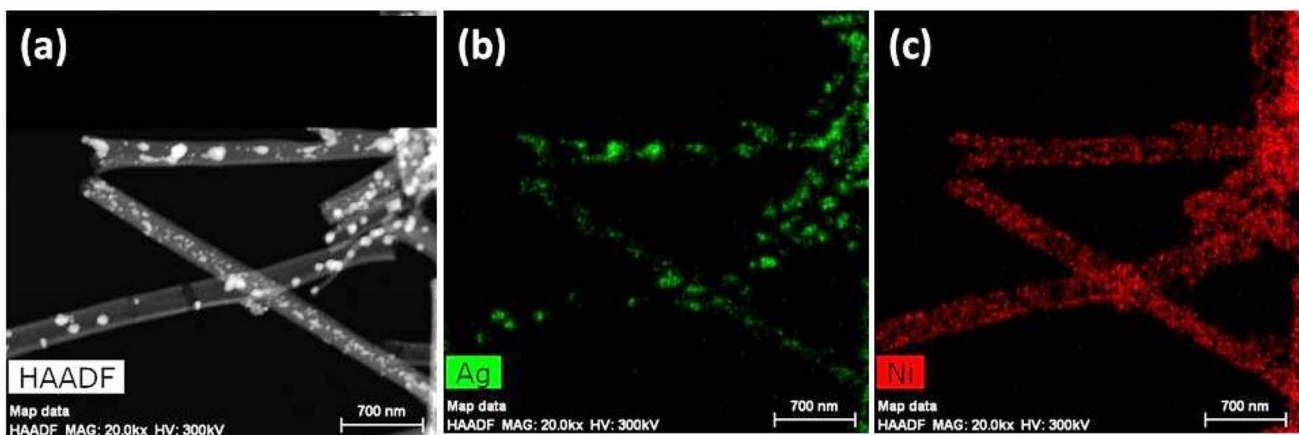
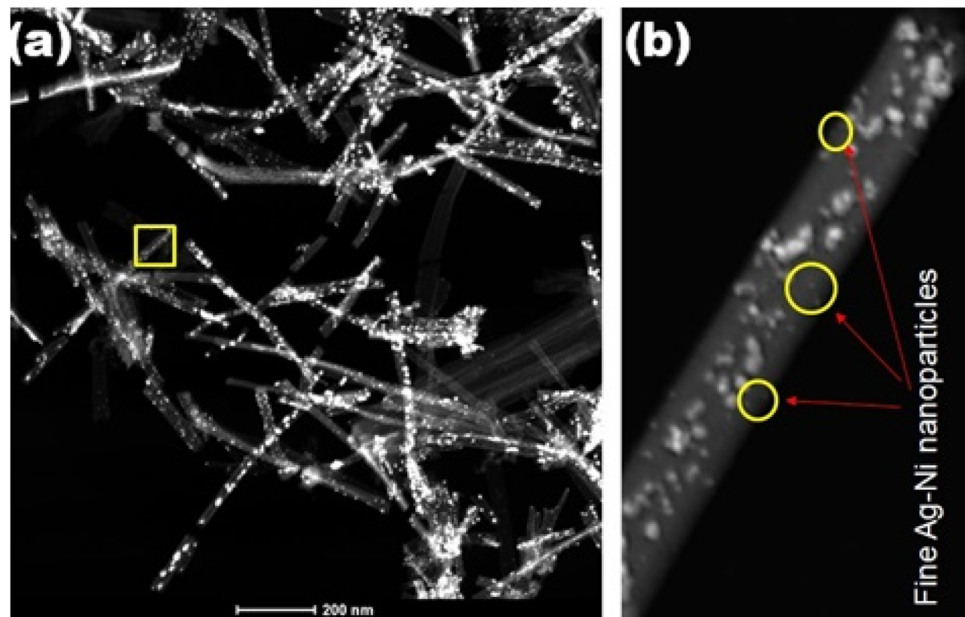
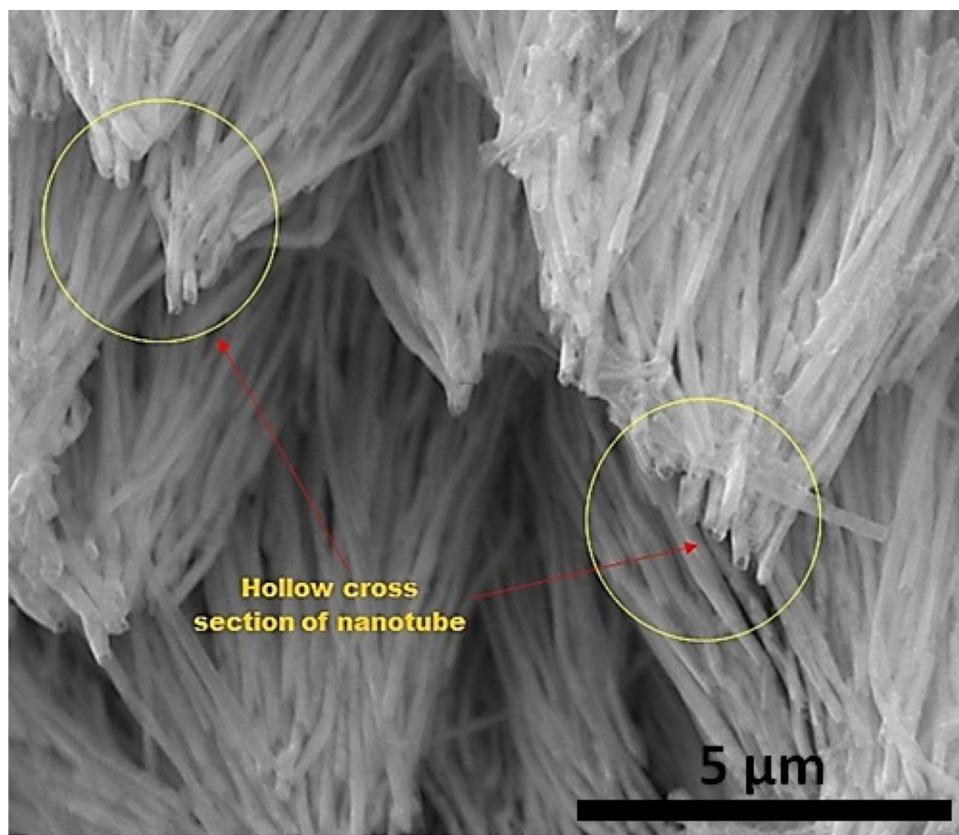


Fig. 5 Results obtained from compositional mapping analysis showing (a) STEM-HAADF images of nanotubes, (b) regions containing Ag, and (c) regions containing Ni atoms

indication that the average atomic number is uniform in any analysis column across the cross section indicating a hollow geometry. If the tubes were filled, then the contrast would increase from the periphery to the center as the amount of material (in the electron beam direction) would increase from the periphery to the center of the nanotube.

A representative SEM micrograph showing hollow cross section of the nanotubes is shown in Fig. 6. Compositional maps disclose coexistence of both Ag and Ni atoms in the nanoparticles and dominant presence of Ni in the matrix phase.

Fig. 6 Representative SEM micrograph showing hollow cross section of the nanotubes



The line profile experiments were conducted at two different regions of the nanotubes (Fig. 7a–c). Figure 7a illustrates the STEM-HAADF image of the region of interest (the nanotube). Figure 7b shows the plots obtained in Ag and Ni characteristic x-ray signals in the EDS spectrum captured from different locations along the line AC, which runs across the nanotube matrix (Fig. 7a). The line profile (Fig. 7b) shows that the EDS counts are present for both Ag and Ni atoms across the nanotube matrix. Presence of strong Ni signals as compared to Ag is mainly attributed to the presence of Ni-rich matrix phase. The line profile analysis in Fig. 7c plots count in the Ag and Ni characteristic x-ray signals in the EDS spectrum obtained from different locations along the line KM, which runs along with the particles distributed in the nanotube matrix. The line profiles in Fig. 7c reveal the signals for both Ag and Ni atoms; however, signals corresponding to Ag atoms are very high, which confirms that the nanoparticles are Ag-rich.

To explore the crystal structure of the nanotubes, a high-resolution TEM bright field images (HRTEM) characterization was executed. Related HRTEM image showing two embedded nanoparticles and the tubular matrix is provided in Fig. 8a. Presence of continuous lattice fringes along particles confirmed that they are crystalline, whereas absence of lattice fringes for the matrix revealed its amorphous nature. The fast Fourier transform (FFT) diffraction pattern of the nanoparticle is shown in the inset in Fig. 8b. The FFT (Fig. 8b) shows that this particle has single-phase solid solution structure as the reflections on the ring belong to one fcc phase (value of d-spacing is 2.28 Å) [10]. This d-spacing value is equal to the d-spacing value for the (111) plane of the Ag–Ni alloy phase [11]. It is observed that one of the embedded particle exhibited multiple twin structure (particle 1), whereas the other particle shows single crystal structure (particle 2). It is noteworthy that the larger size particle shows multiple twin

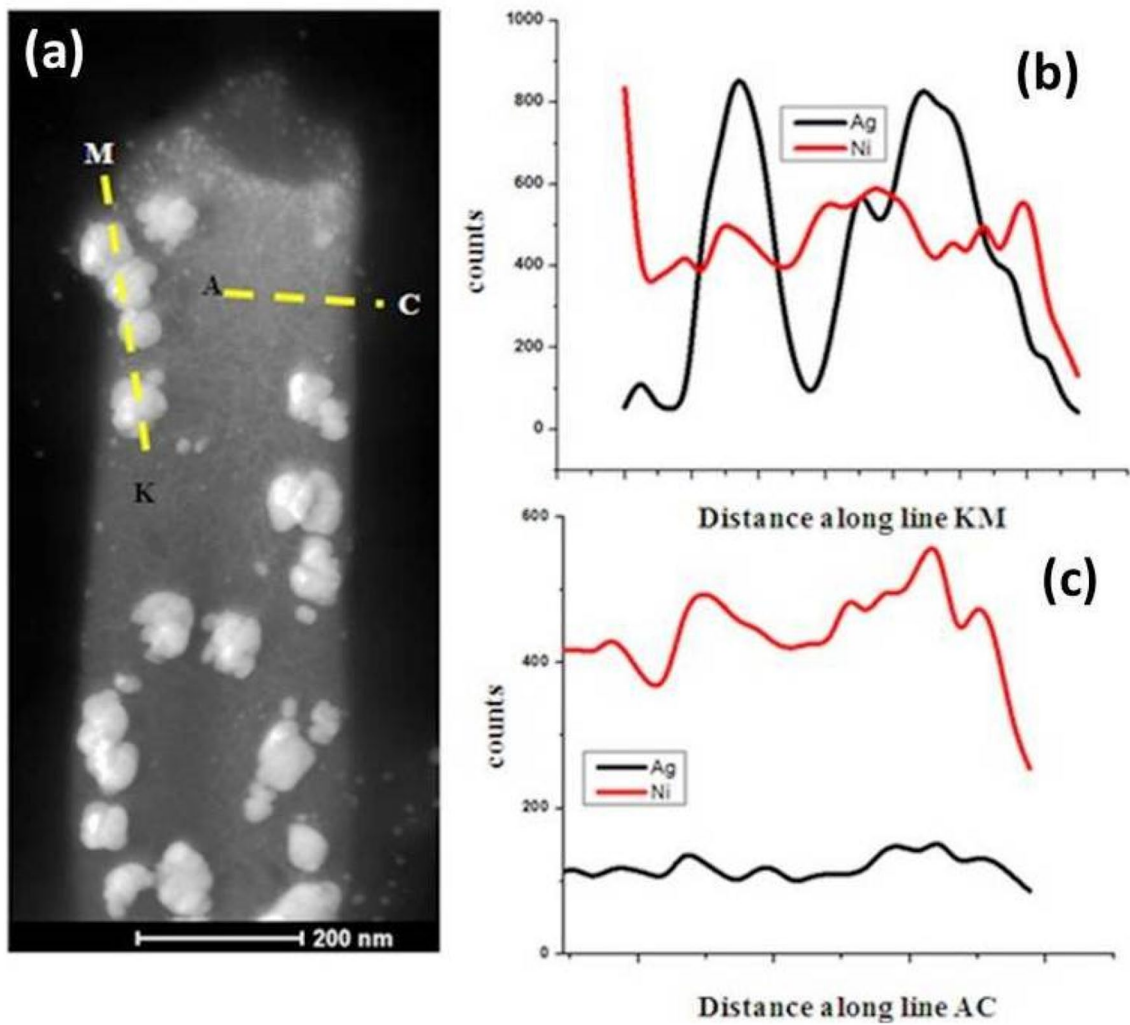


Fig. 7 (a) STEM image (b) plot of counts of Ag and Ni characteristic x-ray signals along the line KM (c) plot of counts of Ag and Ni characteristic x-ray signals along the line AC

structure, whereas smaller particle shows single crystal structure. Figure 9 illustrates more representative HRTEM images of such particles. Multiple twinning structures have been observed in many fcc alloy nanoparticles [12–16]. Selected area electron diffraction pattern (SADP) acquired from several nanoparticles embedded in the nanotube (from a large agglomerate of nanotubes) is provided in Fig. 10. The SAED pattern does not reveal any diffraction signature corresponding to pure Ni or Ni and Ag oxide

phases. r_1 , r_2 , r_3 , and r_4 denote the first four rings present in SAED pattern. It is also worth to notice that the ratio of the d-spacing values ($r_1/r_2 = 1.14$, $r_1/r_3 = 1.64$, $r_1/r_4 = 1.92$, $r_2/r_3 = 1.44$, $r_2/r_4 = 1.66$, $r_3/r_4 = 1.15$) is nearly equivalent to the d-ratio of standard fcc crystal which is possibly Ag [7, 13]. The results obtained from compositional and crystallographic analysis indicate that the nanotube contains crystalline Ag-rich, Ag–Ni solid solution phase nanoparticles distributed in the amorphous matrix.

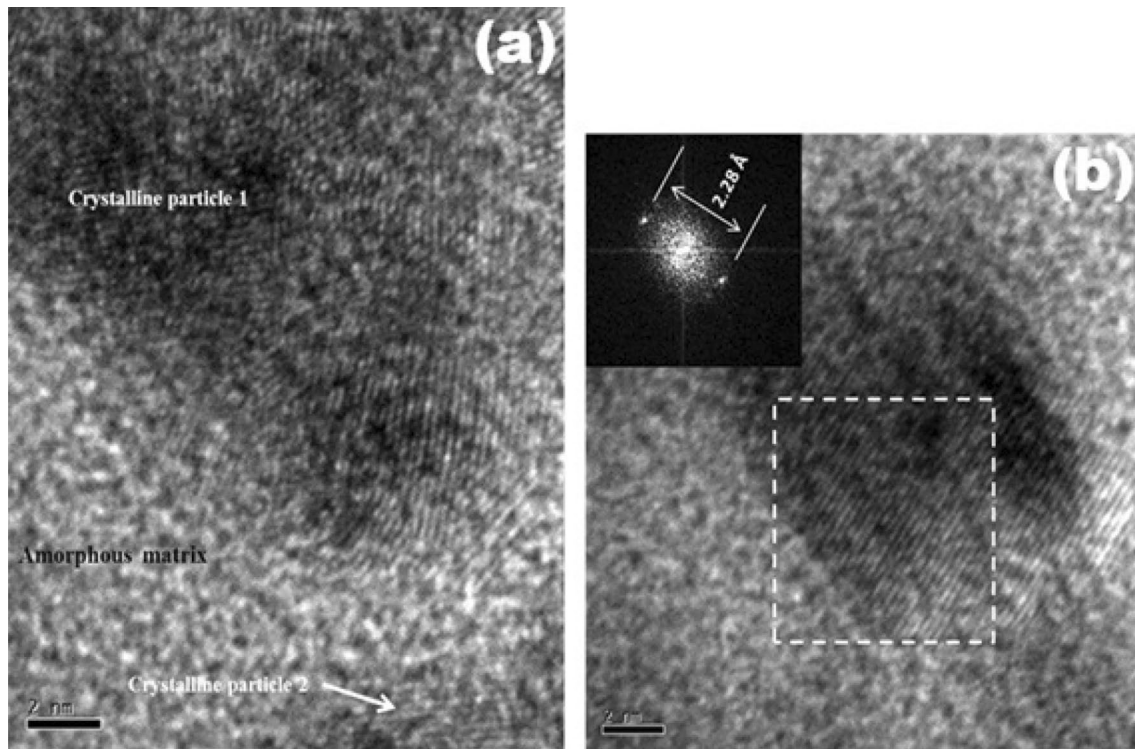


Fig. 8 (a) and (b) HRTEM image of nanoparticles and the matrix in the nanotube microstructure

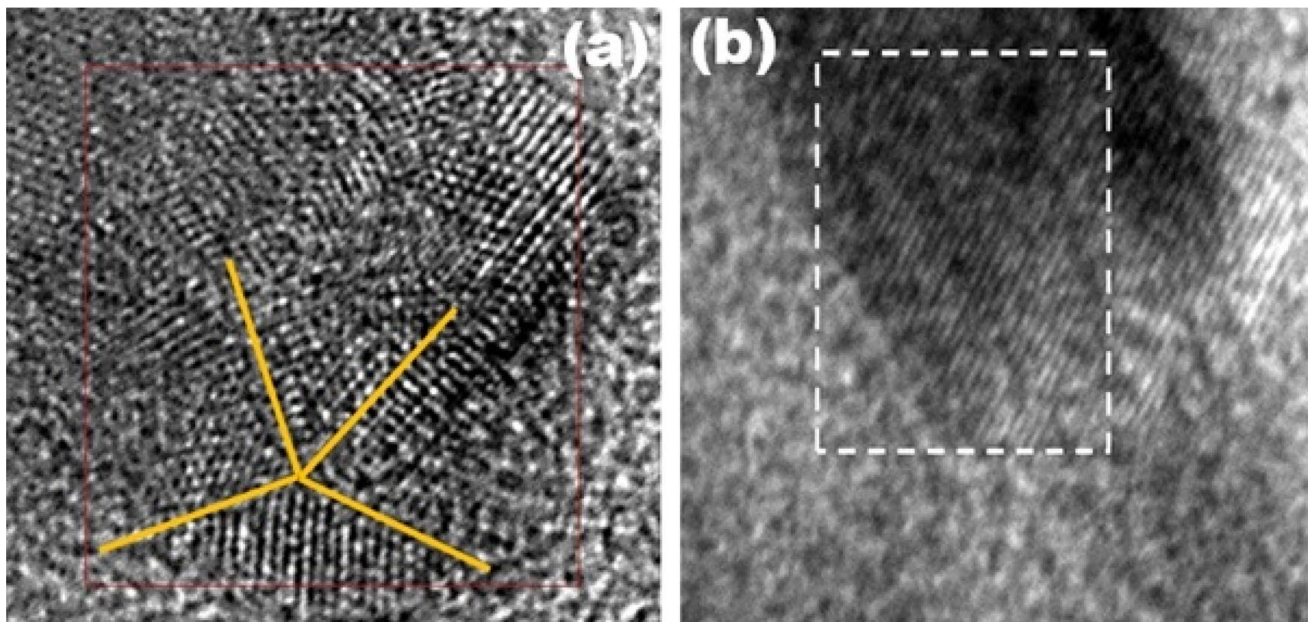


Fig. 9 HRTEM image showing (a) multiple twin structure in larger particles (b) smaller particles showing single crystal structure

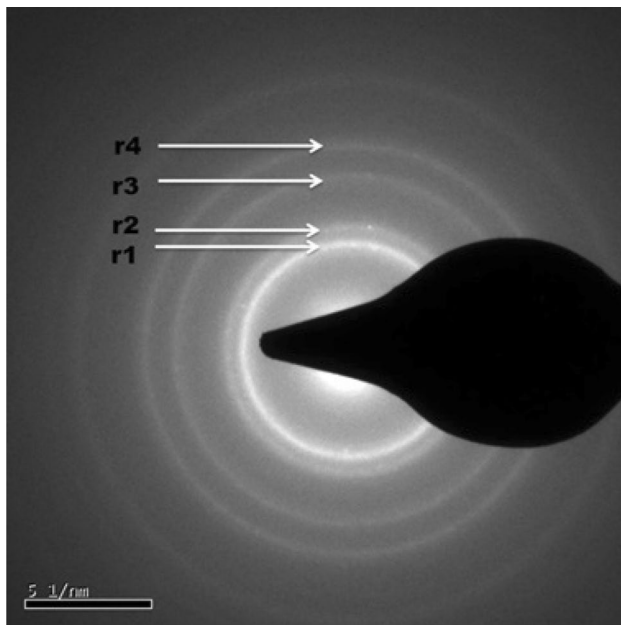


Fig. 10 SAED pattern obtained from nanotubes

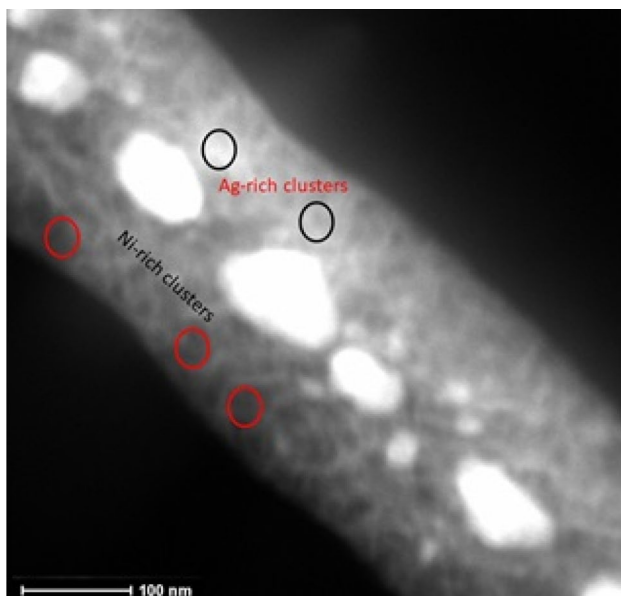


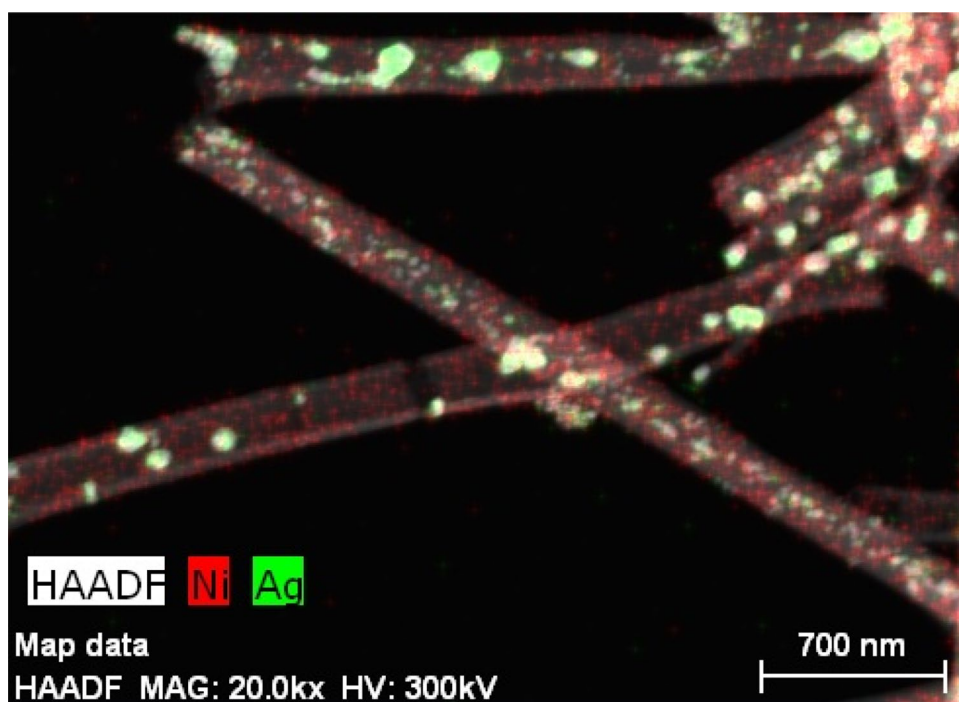
Fig. 11 A high magnification STEM image showing atomic clusters

The size-dependent phase separation of Ag–Ni alloy system has been extensively studied [10, 12]. It is reported that the phase separation occurs by equilibrium process through nucleation [10]. Srivastava et al. have reported the tendency for the formation of solid solution of Ag and Ni atoms at nanoscale. In their work [12], it was shown that only small-sized particles (< 7 nm) form solid solution. For the larger particle, phase separation occurs and a two-phase microstructure consisting of Ag–Ni solid solution and Ag phase is formed. In the present work, it is believed that during the early stage of the electrodeposition process, Ag–Ni nanoparticles are nucleated [10] inside the alumina template. As the deposition process continues, the particles started growing for the sake of minimization of Gibbs free energy of the system [11]. Some of these particles growing larger owing to the formation of multiple twinning structure, which reduces associated strain [12]. It is worth noting [12] that even twinning structures can accommodate limited strain; therefore, after reaching a critical particle size, phase separation happens and Ag-rich and Ni-rich clusters are formed. These clusters of atoms encapsulated the nanoparticles and form the tube matrix. A high magnification STEM image (Fig. 11) and the compositional map (Fig. 12) of representative Ag–Ni nanotube are well supporting this fact.

Conclusion

A two-phase microstructure of Ag–Ni nanotubes was obtained by employing a template-based electrodeposition technique. The microstructure of the as-deposited nanotube consisted of nearly spherical nanoparticles encapsulated in a hollow cylindrical matrix. It is evident from compositional and structural characterization that the particles embedded in the nanotube microstructure contained Ag-rich, Ag–Ni solid solution phase, and the matrix was made up of Ag-rich and Ni-rich clusters. On the basis of the microstructural characterization, a possible mechanism of the formation of the microstructure is provided which involves the nucleation followed by the growth of Ag–Ni nanoparticles inside the alumina template. Some of these particles grow larger by adopting multiple twinning structure and after acquiring a critical size, phase separation occurs, which leads to the formation of Ag-rich and Ni-rich clusters that matured to the nanotube.

Fig. 12 Compositional map of representative Ag–Ni nanotube



Acknowledgements The authors acknowledge the funding received from the SERB Govt. of India.

Compliance with Ethical Standards

Conflict of interest The authors declare that there is no conflict of interest.

References

1. K. Ramachandran, K. Justice Babu, K. Ramachandran, K. Justice Babu, Ni-Co bimetal nanowires filled multiwalled carbon nanotubes for the highly sensitive and selective non-enzymatic glucose sensor applications. *Sci. Rep.* **6**, 36583 (2016). <https://doi.org/10.1038/srep36583>
2. L. Dimesso, G. Miede, H. Fuess, H. Hahn, L. Dimesso, G. Miede, H. Fuess, H. Hahn, Preparation of nanostructured granular Ag–Co and Ag–Fe alloys by gas flow condensation technique. *J. Magn. Mater.* **191**, 162–168 (1999). [https://doi.org/10.1016/S0304-8853\(98\)00326-6](https://doi.org/10.1016/S0304-8853(98)00326-6)
3. C.-C. Lee, D.-H. Chen, C.-C. Lee, D.-H. Chen, Large-scale synthesis of Ni–Ag core–shell nanoparticles with magnetic, optical and anti-oxidation properties. *Nanotechnology*. **17**, 3094 (2006). <https://doi.org/10.1088/0957-4484/17/13/002>
4. H. Guo, Y. Chen, X. Chen, R. Wen, G.-H. Yue, D.-L. Peng, H. Guo, Y. Chen, X. Chen, R. Wen, G.-H. Yue, D.-L. Peng, Facile synthesis of near-monodisperse Ag@ Ni core–shell nanoparticles and their application for catalytic generation of hydrogen. *Nanotechnology*. **22**, 195604 (2011). <https://doi.org/10.1088/0957-4484/22/19/195604>
5. S. Xu, Z.L. Wang, S. Xu, Z.L. Wang, One-dimensional ZnO nanostructures: solution growth and functional properties. *Nano Res.* **4**, 1013–1098 (2011). <https://doi.org/10.1007/s12274-011-0160-7>
6. R.K. Rai, C. Srivastava, R.K. Rai, C. Srivastava, Nonequilibrium microstructures for Ag–Ni nanowires. *Microsc. Microanal.* **21**, 491–497 (2015). <https://doi.org/10.1017/S1431927615000069>
7. C. Srivastava, R.K. Rai, C. Srivastava, R.K. Rai, Transmission electron microscopy study of Ni-rich, Ag–Ni nanowires. *Chem. Phys. Lett.* **575**, 91–96 (2013). <https://doi.org/10.1016/j.cplett.2013.05.011>
8. M. Singleton, P. Nash, M. Singleton, P. Nash, The Ag–Ni (Silver–Nickel) system. *J. Phase Equilibria*. **8**, 119–121 (1987). <https://doi.org/10.1007/BF02873194>
9. S.V. Aert, K.J. Batenburg, M.D. Rossell, R. Erni, G.V. Tendeloo, S.V. Aert, K.J. Batenburg, M.D. Rossell, R. Erni, G.V. Tendeloo, Three-dimensional atomic imaging of crystalline nanoparticles. *Nature*. **470**, 374–377 (2011). <https://doi.org/10.1038/nature09741>
10. G. Radnóczy, E. Bokanyi, Z. Erdélyi, F. Misják, G. Radnóczy, E. Bokanyi, Z. Erdélyi, F. Misják, Size dependent spinodal decomposition in Cu–Ag nanoparticles. *J. Actamat.* **123**, 82–89 (2017). <https://doi.org/10.1016/j.actamat.2016.10.036>
11. C. Srivastava, S. Chithra, K.D. Malviya, S.K. Sinha, K. Chattopadhyay, C. Srivastava, S. Chithra, K.D. Malviya, S.K. Sinha, K. Chattopadhyay, Size dependent microstructure for Ag–Ni nanoparticles. *Acta Mater.* **59**, 6501–6509 (2011). <https://doi.org/10.1016/j.actamat.2011.07.022>
12. C. Srivastava, C. Srivastava, Phase separation by nanoparticle splitting. *Mater. Lett.* **70**, 122–124 (2012). <https://doi.org/10.1016/j.matlet.2011.11.079>
13. H. Hofmeister, H. Hofmeister, Forty years study of fivefold twinned structures in small particles and thin films. *Cryst. Res. Technol.* **33**, 3–25 (1998). [https://doi.org/10.1002/\(SICI\)1521-4079\(1998\)33:1%3c3::AID-CRAT3%3e3.0.CO;2-3](https://doi.org/10.1002/(SICI)1521-4079(1998)33:1%3c3::AID-CRAT3%3e3.0.CO;2-3)
14. V.V. Volkov, G. Van Tendeloo, G.A. Tsirkov, N.V. Cherkashina, M.N. Vargaftik, I.I. Moiseev, V.M. Novotortsev, A.V. Kvit, A.L. Chuvilin, V.V. Volkov, G. Van Tendeloo, G.A. Tsirkov, N.V. Cherkashina, M.N. Vargaftik, I.I. Moiseev, V.M. Novotortsev, A.V. Kvit, A.L. Chuvilin, Long- and short-distance ordering of the

- metal cores of giant Pd clusters. *J. Cryst. Growth.* **163**, 377–387 (1996). [https://doi.org/10.1016/0022-0248\(95\)01008-4](https://doi.org/10.1016/0022-0248(95)01008-4)
15. G. Radnóczy, E. Bokanyi, Z. Erdélyi, F. Misják, G. Radnóczy, E. Bokanyi, Z. Erdélyi, F. Misják, Size dependent spinodal decomposition in Cu-Ag nanoparticles. *Acta Mater.* **123**, 82–89 (2017). <https://doi.org/10.1016/j.actamat.2016.10.036>
 16. T.P. Martin, T. Bergmann, H. Göhlich, T. Lange, T.P. Martin, T. Bergmann, H. Göhlich, T. Lange, Evidence for icosahedral shell structure in large magnesium clusters. *Chem. Phys. Lett.* **176**, 343–347 (1991)

Publisher's Note Springer Nature remains neutral with regard to jurisdictional claims in published maps and institutional affiliations.